RADIO CONSTRAINTS ON LONG-LIVED MAGNETAR REMNANTS IN SHORT GAMMA-RAY BURSTS

The Astrophysical Journal, 831:141 (9pp), 2016 November 10 doi:10.3847/0004-637X/831/2/141

RADIO CONSTRAINTS ON LONG-LIVED MAGNETAR REMNANTS IN SHORT GAMMA-RAY BURSTS

W. Fong[1,4], B. D. Metzger[2], E. Berger[3], and F. Özel[1]
[1] Steward Observatory, University of Arizona, 933 N. Cherry Avenue, Tucson, AZ 85721, USA
[2] Columbia Astrophysics Laboratory, Columbia University, New York, NY 10027, USA
[3] Harvard-Smithsonian Center for Astrophysics, 60 Garden Street, Cambridge, MA 02138, USA
Received 2016 July 1; revised 2016 August 29; accepted 2016 August 29; published 2016 November 3

ABSTRACT

The merger of a neutron star (NS) binary may result in the formation of a rapidly spinning magnetar. The magnetar can potentially survive for seconds or longer as a supramassive NS before collapsing to a black hole if, indeed, it collapses at all. During this process, a fraction of the magnetar's rotational energy of $\sim 10^{53}$ erg is transferred via magnetic spin-down to the surrounding ejecta. The resulting interaction between the ejecta and the surrounding circumburst medium powers a year-long or greater synchrotron radio transient. We present a search for radio emission with the Very Large Array following nine short-duration gamma-ray bursts (GRBs) at rest-frame times of $\approx$1.3–7.6 yr after the bursts, focusing on those events that exhibit early-time excess X-ray emission that may signify the presence of magnetars. We place upper limits of $\lesssim$18–32 μJy on the 6.0 GHz radio emission, corresponding to spectral luminosities of $\lesssim (0.05\text{–}8.3) \times 10^{39}$ erg s^{-1}. Comparing these limits to the predicted radio emission from a long-lived remnant and incorporating measurements of the circumburst densities from broadband modeling of short GRB afterglows, we rule out a stable magnetar with an energy of 10^{53} erg for half of the events in our sample. A supramassive remnant that injects a lower rotational energy of 10^{52} erg is ruled out for a single event, GRB 050724A. This study represents the deepest and most extensive search for long-term radio emission following short GRBs to date, and thus the most stringent limits placed on the physical properties of magnetars associated with short GRBs from radio observations.

Key words: gamma-ray burst: general – stars: neutron – stars: magnetars

1. INTRODUCTION

The merger of two neutron stars (NSs) in a compact binary can result in the formation of a massive NS remnant, which is generally assumed to collapse subsequently to a black hole. Accretion onto the black hole then powers a relativistic transient, a short-duration gamma-ray burst (GRB; Narayan et al. 1992; Ruffert & Janka 1999; Aloy et al. 2005; Rezzolla et al. 2011; Berger et al. 2013; Tanvir et al. 2013; Berger 2014; Ruiz et al. 2016), with a prompt gamma-ray emission duration of $\lesssim$ 2 s. One of the biggest uncertainties in this canonical picture is how long the NS remnant survives prior to collapse. This depends on the mass of the final remnant and the highly uncertain Equation of State (EOS) of dense nuclear matter (Özel et al. 2010, 2016; Lasky et al. 2014; Fryer et al. 2015; Lawrence et al. 2015).

A massive NS remnant, which is supported against gravity exclusively by its differential rotation, is known as a *hypermassive* NS. Somewhat less massive NSs, which can be supported even by their solid body rotation, are known as *supramassive*. A hypermassive NS can survive for at most a few hundred milliseconds after the merger, before collapsing due to the loss of its differential rotation by internal electromagnetic torques and gravitational wave radiation (e.g., Shibata & Taniguchi 2006). In contrast, supramassive remnants spin-down to the point of collapse through less efficient processes, such as magnetic dipole radiation, and hence can remain stable for $\gtrsim$seconds to minutes. The discovery of NSs with masses $\approx 2\,M_{\odot}$ (Demorest et al. 2010; Antoniadis et al. 2013) places a lower limit on the maximum NS mass, making it likely that the remnants produced in at least some NS mergers are supramassive (e.g., Özel et al. 2010). The mergers of particularly low mass binaries may even produce *indefinitely stable* remnants, from which a black hole never forms (e.g., Giacomazzo & Perna 2013).

The high angular momentum of a merging binary guarantees that the NS remnant will be born rotating rapidly, with a spin period close to the break-up value of $\sim$1 ms. The remnant may also acquire a strong magnetic field, $\gtrsim 10^{14}$–10^{15} G, as a result of shear-induced instabilities and dynamo activity (Duncan & Thompson 1992; Usov 1992; Price & Rosswog 2006; Zrake & MacFadyen 2013). Such a supramassive "magnetar" remnant possesses a reservoir of rotational energy up to $\approx 10^{53}$ erg (Metzger & Bower 2014; Metzger et al. 2015), which is not available in cases where the NS promptly collapses to a black hole. Through its magnetic dipole spin-down, a magnetar remnant serves as a continuous power source, with the exact evolution of its spin-down luminosity dependent on the birth period and dipole magnetic field strength of the remnant (Zhang & Mészáros 2001; Metzger et al. 2008; Bucciantini et al. 2012; Siegel et al. 2014; Siegel & Ciolfi 2016).

Metzger et al. (2008) showed that the ongoing energy input from a long-lived magnetar is well-matched to a puzzling feature that distinguishes a subset of short GRBs: $\approx 1/4$ to $1/2$ of short bursts discovered with the*Swift* satellite (Gehrels et al. 2004) have excess emission in their light curves when compared to the standard synchrotron model for afterglows. Indeed, $\approx$15%–20% of *Swift* short GRBs have prolonged hard X-ray activity for tens to hundreds of seconds following the bursts themselves ("extended emission"; Norris & Bonnell 2006; Perley et al. 2009). Other events have a temporary flattening or "plateau" in the flux decline rate of their X-ray afterglows for $\approx 10^2$–10^3 s after the burst (Margutti et al. 2013; Rowlinson et al. 2013; Lü et al. 2015). Still others have late-time excess X-ray emission on timescales of ~few days (Perley

[4] Einstein Fellow.

et al. 2009; Fong et al. 2014). Other than the anomalous X-ray behavior, there are no obvious differences between these bursts and the normal population of short GRBs in any of their host galaxy properties (Fong et al. 2013), suggesting an origin intrinsic to the burst central engine.

Long-lived magnetar remnants have been commonly invoked to explain the excess emission observed following short GRBs. Several studies have fit magnetar models to short GRBs with extended emission (Gompertz et al. 2013), X-ray and optical plateaus (Rowlinson et al. 2010a, 2013; Gompertz et al. 2015; Lü et al. 2015), and late-time excess emission (Fan et al. 2013; Fong et al. 2014), resulting in inferred spin periods of ≈1–10 ms and large magnetic fields of $\approx(2\text{–}40)\times10^{15}$ G. As an alternative to the magnetar model, other energy sources remain energetically viable: most notably, late-time "fall-back" accretion onto the remnant black hole (Rosswog 2007; Kumar et al. 2008; Cannizzo et al. 2011). In order to substantiate the magnetar scenario for this subset of short GRBs, and also provide crucial insight on the NS EOS, it is necessary to test additional predictions of the magnetar model.

Synchrotron radio emission is expected from the interaction of the ejecta in an NS merger and the surrounding circumburst medium (Nakar & Piran 2011), similar to a young supernova remnant. Metzger & Bower (2014) pointed out that the radio brightness of this interaction would be significantly enhanced in the case of a supramassive or stable magnetar remnant, due to the additional energy imparted to the ejecta by the injected rotational energy, which can exceed that of the dynamical ejecta by three or four orders of magnitude. Since there is substantial observational evidence linking short GRBs to NS mergers (Berger et al. 2013; Fong & Berger 2013; Tanvir et al. 2013; Berger 2014), radio observations following short GRBs offer an independent way to explore the existence of long-lived (supramassive or stable) magnetar remnants. Using radio observations of seven short GRBs on ∼1–3 year timescales, Metzger & Bower (2014) placed constraints on the circumburst density of $\lesssim$0.1–1 cm^{-3}, assuming an energy reservoir of 3×10^{52} erg. Similarly, Horesh et al. (2016) analyzed two bursts and placed limits of $\lesssim$0.001–5 cm^{-3} depending on the value of the assumed ejecta mass, and assumed the same energy of 3×10^{52} erg.

Here, we present radio observations of nine short GRBs on rest-frame timescales of ∼2–8 yr after the bursts, focusing on those events that exhibit excess X-ray emission at early times that may signify the presence of magnetars. This sample represents the largest and deepest survey for long-timescale radio emission of short GRBs to date, and provides a unique test of the magnetar model. We utilize this data set to constrain the presence of magnetars formed as a result of the mergers. In Section 2, we outline the sample and radio observations. In Section 3, we describe the magnetar model and in Section 4, we present the analysis and results, including the constraints on the magnetar rotational energies and environment circumburst densities. In Section 5, we compare this work to previous studies of emission from magnetars in short GRBs, and we conclude in Section 6.

2. OBSERVATIONS

2.1. Sample

We select all short GRBs with sub-arcsecond localization, spectroscopic redshifts, and sky locations observable with the Very Large Array (VLA). We further require that the events have pre-existing observations that indicate unusual behavior potentially attributed to a remnant magnetar: extended emission, X-ray plateau, or a late-time X-ray excess. These selection criteria limit our sample to nine events (Table 1). In our sample, two events have extended emission, six have X-ray plateaus, and one has a possible late-time excess or plateau.

We note that for each burst, the redshifts are derived from the host galaxy. With the exception of GRB 090515, all bursts in our sample have extremely robust associations to their host galaxies, with probabilities of chance coicidence ($P_{\rm cc}$) of $\lesssim$1%. For GRB 090515, the most probable host galaxy has $z=0.403$ with $P_{\rm cc}\approx15\%$, while the next most probable host galaxy has $z=0.626$ with $P_{\rm cc}\approx25\%$ (Berger 2010; Tunnicliffe et al. 2014). We assume $z=0.403$ as the redshift of this burst throughout the paper. However, if $z=0.626$ is in fact the true redshift of GRB 090515, then the luminosity limit is less stringent, with $\nu L_\nu\lesssim2.3\times10^{39}$ erg s^{-1}. We note that the assumption of this redshift does not affect the overall conclusions of our study.

2.2. VLA Observations

We observed the positions of nine short GRBs with the Karl G. Jansky Very Large Array (VLA) from 2015 February 21 to March 6 UT (Table 1; Program 15A-246). For each burst, we obtained 1 hr of observations in B configuration at a mean frequency of 6.0 GHz (lower and upper side-bands centered at 4.9 and 7.0 GHz). We follow standard procedures in the Astronomical Image Processing System (AIPS; Greisen 2003, p. 109) for data calibration and analysis, using 3C 48 and 3C 286 for flux calibration, and standard sources as part of the VLA calibrator manual[5] for gain calibration. We do not detect any source in or around the positions of the GRBs. To obtain 3σ upper limits on the flux density, F_ν, we use AIPS/IMSTAT on source-free regions surrounding the GRB positions. The 6.0 GHz upper limits are listed in Table 1. The limits span a range, $F_\nu\lesssim$ 18–32 μJy with a median of $F_\nu\lesssim22$ μJy.

3. MAGNETAR MODEL

Simulations of binary NS mergers find the dynamical ejection of $\sim0.01\,M_\odot$ of material (Rosswog et al. 1999; Hotokezaka et al. 2013a; Kyutoku et al. 2015; Radice et al. 2016), while a comparable or greater amount of mass may be lost in outflows from the remnant accretion disk (Metzger et al. 2009; Fernández & Metzger 2013; Just et al. 2015). In the case of a long-lived NS remnant, the disk wind ejecta mass can approach the total disk mass of $\approx0.1\,M_\odot$ (Metzger & Fernández 2014). A high ejecta mass of $\sim0.03\text{–}0.08\,M_\odot$ was also inferred based on modeling the kilonova emission from the short GRB 130603B (Berger et al. 2013; Hotokezaka et al. 2013b; Tanvir et al. 2013).

In the case of a long-lived magnetar, a significant fraction of the magnetar's rotational energy can be imparted to the dynamical and disk wind ejecta, accelerating it to mildly relativistic speeds (Metzger & Bower 2014; Metzger & Piro 2014). The deceleration of this fast material by its shock interaction with the circumburst medium produces synchrotron emission peaking at MHz to GHz frequencies (Nakar & Piran 2011; Metzger & Bower 2014; Hotokezaka &

[5] https://science.nrao.edu/facilities/vla/observing/callist

Table 1
Log of VLA 6.0 GHz Observations

GRB	z	UT Date	$\delta t_{\rm rest}$ (yr)	F_ν (μJy)	νL_ν (erg s^{-1})	X-ray Behavior	Reference[a]
GRB 050724A	0.257	2015 Feb 22.472	7.629	<22.1	2.7×10^{38}	Extended emission[b]	1
GRB 051221A	0.546	2015 Feb 22.718	5.936	<19.5	1.4×10^{39}	Plateau	2
GRB 070724A	0.457	2015 Feb 21.058	5.206	<19.1	9.1×10^{38}	Plateau	3
GRB 080905A	0.122	2015 Feb 23.723	5.769	<22.2	5.2×10^{37}	Plateau	4
GRB 090510	0.903	2015 Mar 6.625	3.062	<26.5	6.6×10^{39}	Extended emission[b]	5
GRB 090515	0.403	2015 Mar 2.427	4.135	<22.7	8.0×10^{38}	Plateau	6
GRB 100117A	0.915	2015 Feb 27.674	2.671	<32.0	8.3×10^{39}	Plateau[c]	7
GRB 101219A	0.718	2015 Feb 24.011	2.437	<17.5	2.5×10^{39}	Plateau	8
GRB 130603B	0.356	2015 Mar 5.451	1.292	<20.6	5.4×10^{38}	Late-time excess/Plateau[d]	9–10

Notes. Upper limits correspond to 3σ confidence.
[a] References for redshifts: (1) Berger et al. (2005), (2) Soderberg et al. (2006), (3) Berger (2009), (4) Rowlinson et al. (2010b), (5) McBreen et al. (2010), (6) Berger (2010), (7) Fong et al. (2011), (8) Fong et al. (2013), (9) Cucchiara et al. (2013), (10) de Ugarte Postigo et al. (2014).
[b] The combined γ-ray and X-ray light curves of GRBs 050724A and 090510 have also been fit with an "internal plateau" model (Lü et al. 2015).
[c] The X-ray afterglow of GRB 100117A also exhibited flaring activity (Margutti et al. 2011).
[d] The late-time X-ray afterglow of GRB 130603B has been explained as an excess relative to the broadband (radio and optical) afterglows (Fong et al. 2014). Alternatively, the X-ray afterglow alone fits well, with a standard "plateau" extending to ≈1000 s (de Ugarte Postigo et al. 2014).

Piran 2015). The synchrotron model provides a mapping from the flux densities to physical parameters of the magnetar and circumburst environment: the magnetar's rotational energy ($E_{\rm rot}$), ejecta mass ($M_{\rm ej}$), circumburst density (n), fractions of post-shock energy in radiating electrons (ϵ_e) and magnetic fields (ϵ_B), and the electron power-law distribution index (p) that describes the input distribution of electrons with $N(\gamma) \propto \gamma^{-p}$.

In the radio band, the synchrotron spectrum is characterized by two break frequencies, the maximum frequency (ν_m) and the self-absorption frequency (ν_a). Here, we assume that the observing frequency is greater than both of the break frequencies, such that $\nu_{\rm obs} > \nu_m$, ν_a, as is generally satisfied at $\nu_{\rm obs} = 6$ GHz (Nakar & Piran 2011). In this regime, the observed flux peaks at a characteristic deceleration timescale, $t_{\rm dec}$, by which time the ejecta transfers most of its energy to the surrounding medium. This timescale is given by (Nakar & Piran 2011)

$$t_{\rm dec} \approx 300 E_{\rm rot,52}^{-1/2} M_{\rm ej,-2}^{5/6} n^{-1/3} \ {\rm days} \quad (1)$$

where $E_{\rm rot,52}$ is the energy in units of 10^{52} erg, $M_{\rm ej,-2}$ is the ejecta mass in units of $0.01\,M_\odot$, and n is the density in cm^{-3}. The corresponding peak flux density is (Nakar & Piran 2011)

$$F_{\nu,{\rm obs,pk}} \approx C E_{52}^{\frac{5p-3}{4}} M_{\rm ej,-2}^{\frac{5p-7}{4}} n^{\frac{p+1}{4}} \epsilon_{B,-1}^{\frac{p+1}{4}} \epsilon_{e,-1}^{p-1} d_{L,27}^{-2} \nu_{\rm obs,6}^{-\frac{p-1}{2}} \ \mu{\rm Jy}, \quad (2)$$

where the microphysical parameters $\epsilon_{e,-1}$ and $\epsilon_{B,-1}$ are in units of 0.1, $d_{L,27}$ is the luminosity distance in units of 10^{27} cm, $\nu_{\rm obs,6}$ is the observing frequency in units of 6.0 GHz, and C is a normalization constant, $3 \times 10^5 \times 1.1^{\frac{5p-7}{2}} \times 4.3^{-\frac{p-1}{2}}$. For $\nu_{\rm obs} > \nu_m$, ν_a, the observed flux evolves as

$$F_{\nu,{\rm obs}} = \begin{cases} F_{\nu,{\rm obs,pk}} \left(\dfrac{t}{t_{\rm dec}}\right)^3 & t < t_{\rm dec} \\ F_{\nu,{\rm obs,pk}} \left(\dfrac{t}{t_{\rm dec}}\right)^{-\frac{15p-21}{10}} & t \geqslant t_{\rm dec} \end{cases} \quad (3)$$

where t is the rest-frame time after the burst in days.

4. ANALYSIS AND RESULTS

4.1. Light Curves

Using Equations (1)–(3), we calculate a suite of model light curves for a range of magnetar energies, ejecta masses, and circumburst densities. For the magnetar energy, we consider the maximum available rotational energy of 10^{53} erg, corresponding to a stable or nearly stable magnetar with a relatively low mass, i.e., $M_{\rm ns} \lesssim 2.2\,M_\odot$ (Metzger et al. 2015). We also consider a more conservative energy of 10^{52} erg, which corresponds to the rotational energy that is removed prior to black hole formation for a supramassive NS with mass ≈10% higher than the maximum mass of a non-rotating NS, i.e., $M_{\rm ns} \approx 2.5\,M_\odot$ (Metzger et al. 2015). A lower energy of $\lesssim 10^{53}$ erg could also account for cases in which energy is lost due to gravitational wave emission; however, we think this scenario is unlikely and discuss this further in Section 5.

Motivated by numerical simulations showing that long-lived merger remnants eject a high percentage, $\gtrsim$30%, of the remnant accretion disk mass (Metzger & Fernández 2014), we consider fiducial values for the ejecta mass of $0.03\,M_\odot$ and $0.1\,M_\odot$. Short GRBs explode in low-density environments, with a median circumburst density of $\approx 4 \times 10^{-3}$ cm^{-3} (Fong et al. 2015); thus we consider a range of circumburst densities over 10^{-4}–1 cm^{-3}. We fix the value of the power-law index p to the median of the short GRB population, $p = 2.4$ (Fong et al. 2015), $\epsilon_e = \epsilon_B = 0.1$, and $\nu_{\rm obs} = 6.0$ GHz. The resulting light curves are shown in Figure 1. To compare the model light curves to the observations, we use the luminosity distance and redshift of each burst to convert the radio flux densities to luminosity and the observed time to rest-frame time after the burst ($\delta t_{\rm rest}$). The data are shown in Figure 1 and listed in Table 1.

Our observations span $\delta t_{\rm rest} \approx 1.3$–7.6 yr and the luminosity limits range between $\nu L_\nu \lesssim (0.05$–$8.3) \times 10^{39}$ erg s^{-1} (Table 1 and Figure 1). The brightest models are for $E_{\rm rot} = 10^{53}$ erg and $M_{\rm ej} = 0.03\,M_\odot$, and the timing of the observations is well-matched to the deceleration timescale for the low-density models, $t_{\rm dec} \approx 3$–14 yr for $n = 10^{-4}$–10^{-2} cm^{-3} (Equation (1)). Consequently, the observations provide the most stringent limits on the circumburst densities, and require

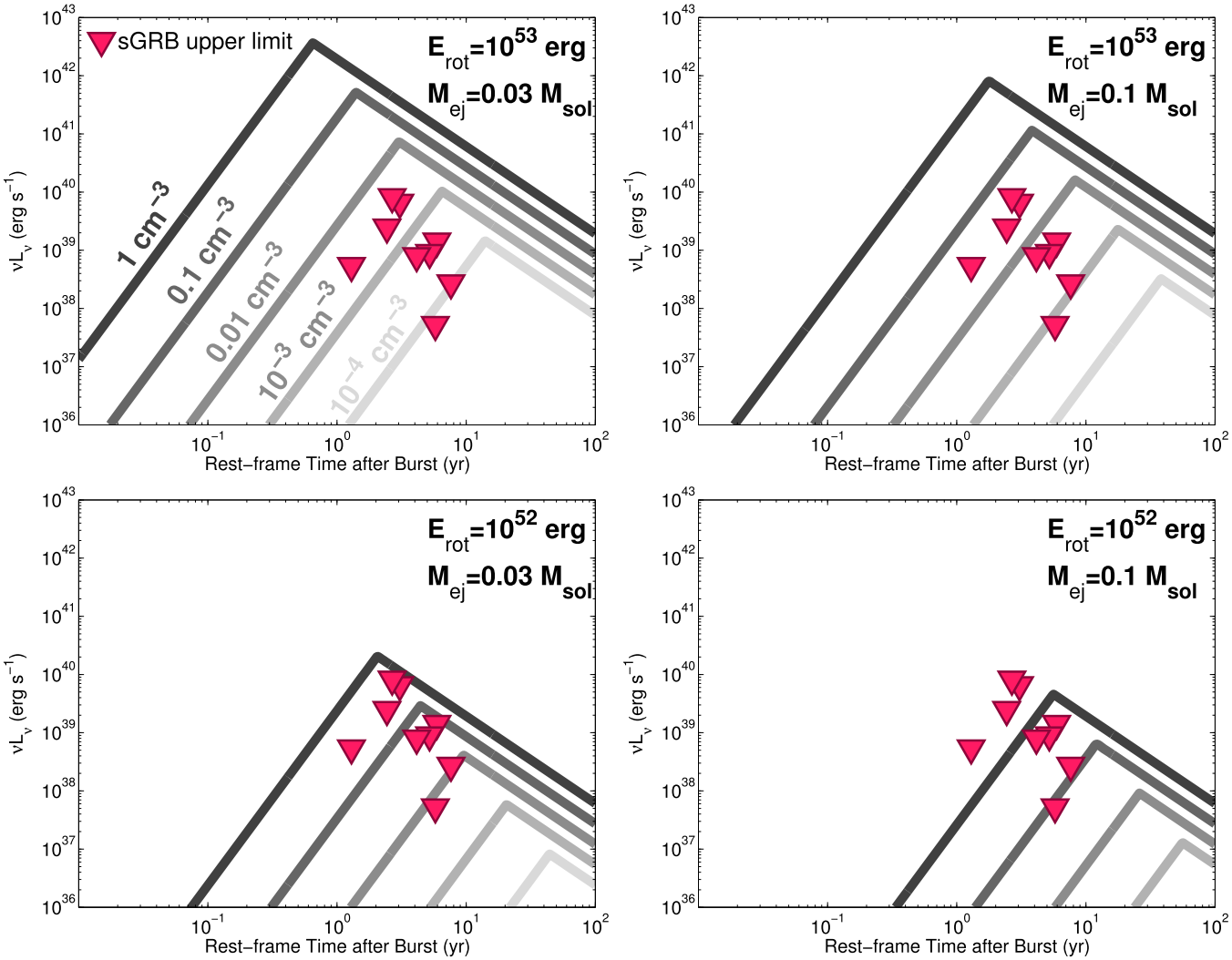

Figure 1. 6.0 GHz luminosity upper limits placed by VLA observations at the positions of nine short GRBs (red triangles), where the limits correspond to 3σ confidence. Also shown are light curve models at 6.0 GHz for varying values of circumburst density (10^{-4}–1 cm^{-3}; gray curves), magnetar rotational energy (10^{52} erg and 10^{53} erg), and ejecta masses (0.03 $M_\odot$ and 0.1 $M_\odot$). These models assume $p = 2.4$ and $\epsilon_e = \epsilon_B = 0.1$. A comparison of the VLA observations to the brightest models (10^{53} erg, $M_{\rm ej} = 0.03\,M_\odot$) requires that the circumburst densities be $\lesssim$(0.09–5) $\times$ 10^{-3} cm^{-3} to accommodate a 10^{53} erg magnetar. Similarly, a comparison to the faintest models (10^{52} erg, $M_{\rm ej} = 0.1\,M_\odot$) contrains the circumburst densities to $\lesssim$0.1–5 cm^{-3}.

that $n \lesssim (0.091\text{–}4.8) \times 10^{-3}\,{\rm cm}^{-3}$ for such a magnetar to be present. However, for a higher ejecta mass of $0.1\,M_\odot$, the deceleration timescale is prolonged by a factor of $\approx$3 (Equation (1)) and the observations are primarily sensitive to the rising portion of the light curves for the lower-density models. We therefore find less stringent circumburst density constraints of $n \lesssim (1.0\text{–}55) \times 10^{-3}\,{\rm cm}^{-3}$ (Figure 1).

Lowering the energy by a factor of 10 to $E_{\rm rot} = 10^{52}$ erg lowers the peak flux by two orders of magnitude, and prolongs the deceleration time by a factor of $\approx$3 for a given ejecta mass. For $E_{\rm rot} = 10^{52}$ erg and $M_{\rm ej} = 0.03\,M_\odot$, the time of observations are similar to the deceleration timescale for the higher-density models, and the density constraints are $n \lesssim (0.96\text{–}47) \times 10^{-2}\,{\rm cm}^{-3}$. The faintest models are for 10^{52} erg and $M_{\rm ej} = 0.1\,M_\odot$; the circumburst density requirements are $n \lesssim 0.11\text{–}5.9\,{\rm cm}^{-3}$.

Overall, considering a magnetar that injects 10^{53} erg of rotational energy, our observations uniformly rule out models for $n \gtrsim 4.8 \times 10^{-3}\,{\rm cm}^{-3}$ ($n \gtrsim 0.06\,{\rm cm}^{-3}$) for an ejecta mass of $0.03\,M_\odot$ ($0.1\,M_\odot$). Similarly, in the more conservative case of 10^{52} erg of energy output, the observations rule out models for $n \gtrsim 0.47\,{\rm cm}^{-3}$ ($\gtrsim 5.9\,{\rm cm}^{-3}$) for an ejecta mass of $0.03\,M_\odot$ ($0.1\,M_\odot$).

4.2. Maximum Magnetar Energy

To constrain the joint rotational energy–circumburst density parameter space with the VLA observations, we use Equations (2) and (3) and the data in Table 1 to obtain expressions for energy as a function of circumburst density. For each burst, we use the upper limits on the flux density to calculate an upper limit on the combination of rotational energy and circumburst density (Equations (2)–(3)). We assume the same fiducial values for p and ϵ_e as in Section 4.1, and consider three values for ϵ_B: 10^{-4}, 0.01, and 0.1. The resulting upper limits on the parameter space are shown for $M_{\rm ej} = 0.03\,M_\odot$ and $0.1\,M_\odot$ in Figures 2 and 3, respectively. The bend in each constraint represents the different behavior before and after the deceleration time.

Additionally, broadband modeling of the afterglow emission provides vital measurements of the circumburst density, which

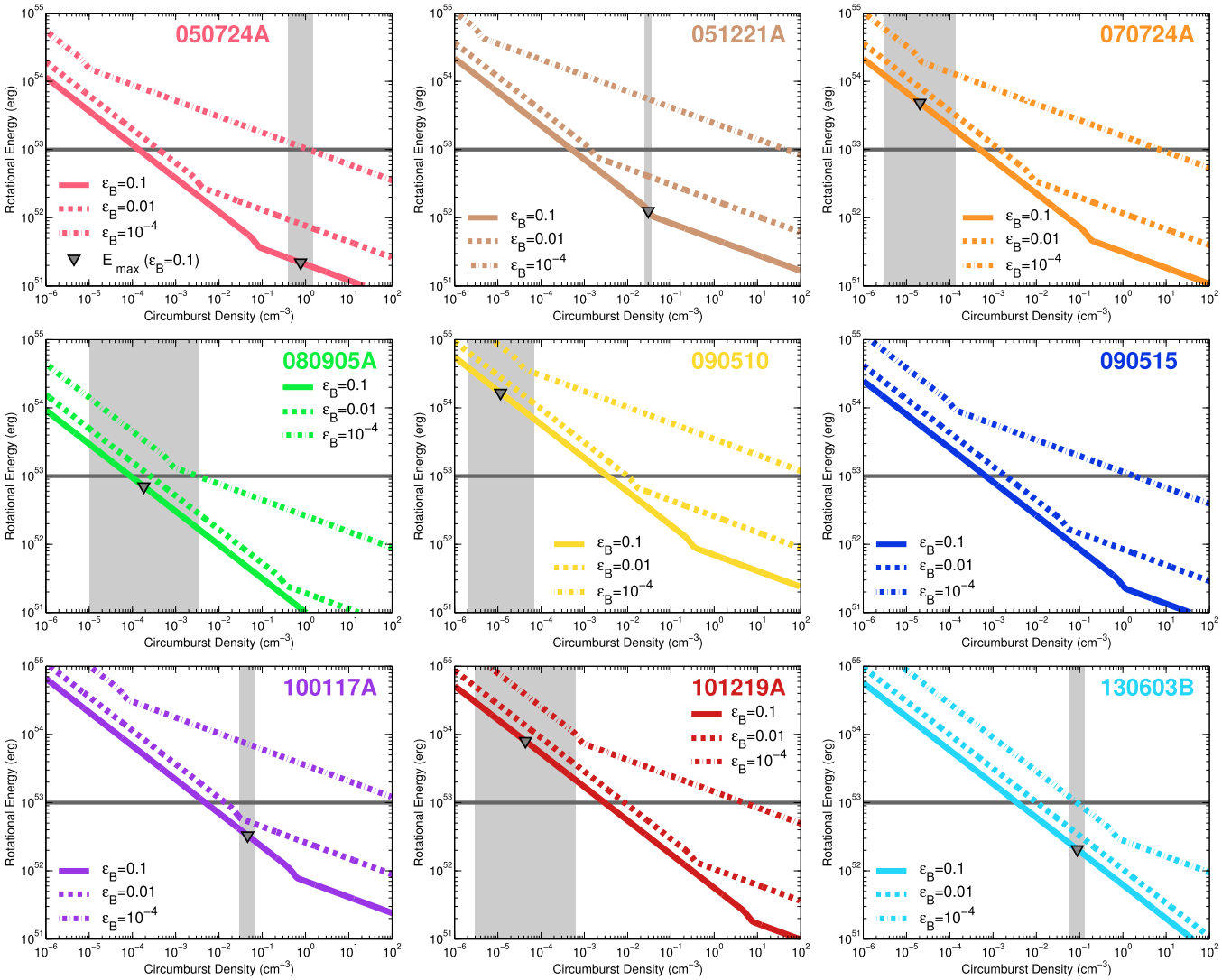

Figure 2. Constraints on the rotational energy–circumburst density parameter space from VLA observations for the nine short GRBs in our sample. Constraints are shown for $M_{\rm ej} = 0.03\,M_\odot$ and $\epsilon_B = 0.1$, 0.01, and 10^{-4} (solid, dashed, and dotted–dashed curves, respectively). In each panel, the curves represent upper limits on the parameter space, where the region below each curve is allowed and the region above is ruled out. Light gray regions represent 1σ ranges of allowed circumburst densities independently determined from afterglow observations for $\epsilon_B = 0.1$ (Fong et al. 2015); there is not enough information to constrain the circumburst density of GRB 090515. The average maximum value of the rotational energy constrained by the observations, $E_{\rm max}$, at $\epsilon_B = 0.1$ is denoted by a gray triangle, corresponding to the values in Table 2. A gray horizonal line shows the maximum extractable rotational energy of a $\sim$2.2 $M_\odot$ magnetar of 10^{53} erg. The observations can rule out the presence of a $\sim$2.2 $M_\odot$ magnetar for GRBs 050724A, 051221A, 080905A, 100117A, and 130603B.

can be used as independent constraints on the allowed parameter space. We collect the inferred circumburst densities for eight bursts from Fong et al. (2015); there is not enough information to constrain the circumburst density of GRB 090515. These values are listed in Table 2 and shown in Figures 2–3, where the ranges shown for each region denote the 1σ uncertainty. Comparing the models over the range of densities allowed by afterglow observations gives an upper limit on the energy of a magnetar remnant, $E_{\rm max}$, listed in Table 2 for both ejecta masses.

The maximum allowed energies are uniformly lower by a factor of $\approx$3 for the smaller ejecta mass. For the four bursts with relatively well-measured densities, GRBs 050724A, 051221A, 100117A, and 130603B, we can rule out the presence of a magnetar with $E_{\rm rot} = 10^{53}$ erg for both ejecta masses. The deepest constraints are for GRB 050724A, for which we can place limits of $E_{\rm max} \approx (2\text{–}5) \times 10^{51}$ erg, two orders of magnitude below the rotational energy of a stable $\sim$2.2 $M_\odot$ magnetar (Table 2; Metzger et al. 2015). Three of the remaining bursts, GRBs 070724A, 090510, and 101219A, have relatively low and uncertain inferred circumburst densities of $\lesssim 10^{-3}$ cm^{-3}; thus the constraints on energy are less stringent, and we cannot rule out the presence of a magnetar with $E_{\rm rot} = 10^{53}$ erg. Finally, for GRB 080905A, a 10^{53} erg magnetar can be ruled out for the smaller ejecta mass only (Table 2 and Figures 2–3). If we consider the conservative case of $E_{\rm rot} = 10^{52}$ erg, only the observations for GRB 050724A can rule out the presence of such a magnetar.

5. DISCUSSION

Prior to this effort, only two attempts have been made to search for radio emission following short GRBs on timescales of $\sim$years. Metzger & Bower (2014) used the VLA (prior to the 2010 upgrade) to observe the fields of seven short GRBs, half of which had extended emission in the X-ray band. The

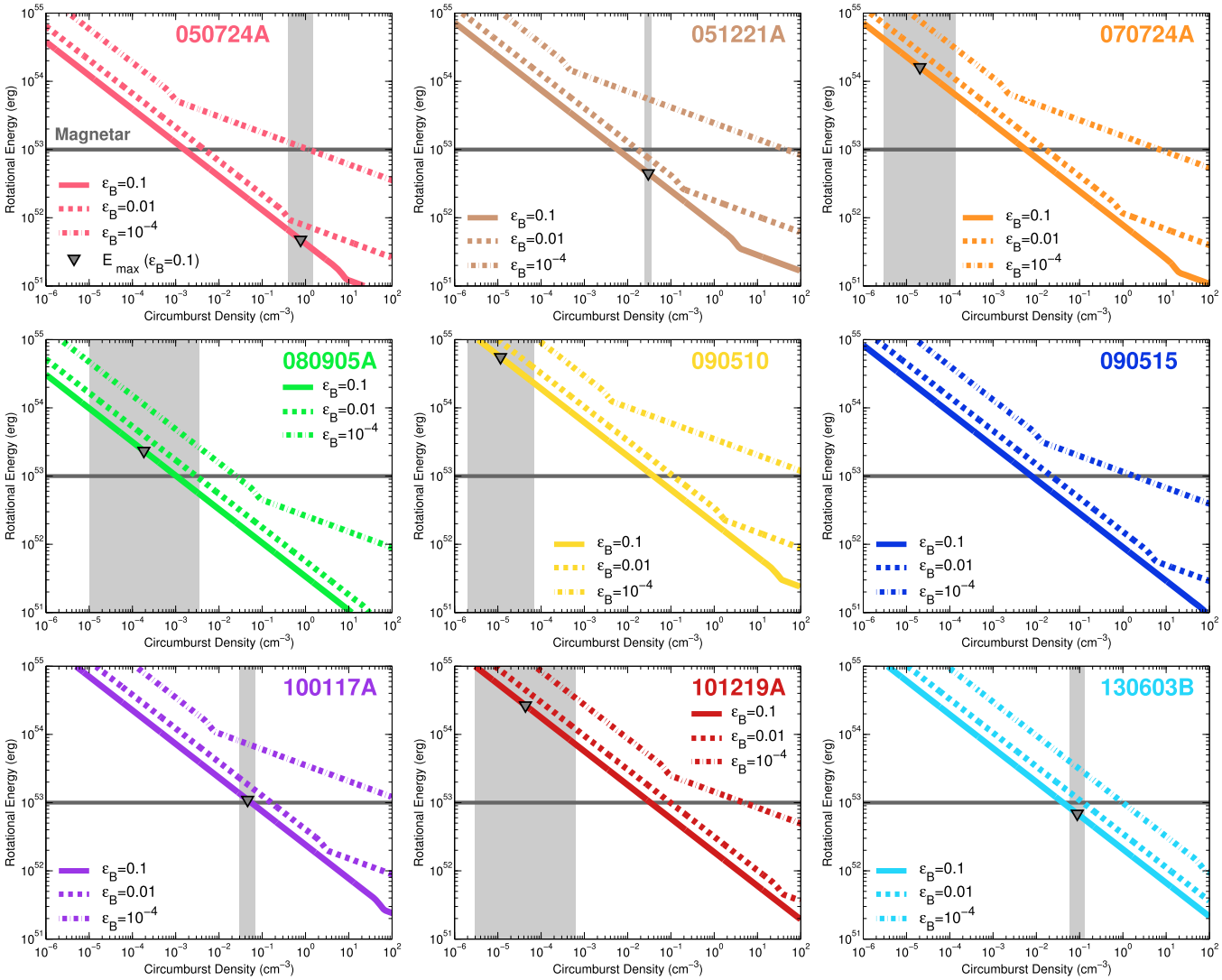

Figure 3. Same as for Figure 2 but for $M_{\rm ej} = 0.1\,M_\odot$. The observations can rule out the presence of a $\sim$2.2 $M_\odot$ magnetar for GRBs 050724A, 051221A, 100117A, and 130603B.

Table 2
Constraints on Magnetar Properties

GRB	Circumburst Density[a] ($\rm cm^{-3}$)	$E_{\rm max}$[b] ($M_{\rm ej} = 0.03\,M_\odot$) (erg)	$E_{\rm max}$[b] ($M_{\rm ej} = 0.1\,M_\odot$) (erg)
GRB 050724A	$0.89^{+0.58}_{-0.49}$	$2.2^{+0.36}_{-0.31} \times 10^{51}$	$4.7^{+1.8}_{-1.3} \times 10^{51}$
GRB 051221A	$0.03^{+0.006}_{-0.005}$	$1.3^{+0.19}_{-0.17} \times 10^{52}$	$4.5^{+0.43}_{-0.39} \times 10^{52}$
GRB 070724A	$1.9^{+12}_{-1.6} \times 10^{-5}$	$4.8^{+7.6}_{-3.0} \times 10^{53}$	$1.6^{+2.5}_{-0.98} \times 10^{54}$
GRB 080905A	$1.3^{+33}_{-1.2} \times 10^{-4}$	$7.0^{+23}_{-5.4} \times 10^{52}$	$2.3^{+7.5}_{-1.8} \times 10^{53}$
GRB 090510	$1.2^{+5.5}_{-1.0} \times 10^{-5}$	$1.7^{+2.3}_{-9.6} \times 10^{54}$	$5.5^{+7.7}_{-3.2} \times 10^{54}$
GRB 090515	…	…	…
GRB 100117A	$0.04^{+0.03}_{-0.01}$	$3.3^{+0.77}_{-6.2} \times 10^{52}$	$1.1^{+0.26}_{-0.21} \times 10^{53}$
GRB 101219A	$4.6^{+59}_{-4.3} \times 10^{-5}$	$8.0^{+21.8}_{-5.8} \times 10^{53}$	$2.6^{+7.3}_{-1.9} \times 10^{54}$
GRB 130603B	$0.09^{+0.04}_{-0.03}$	$2.1^{+0.44}_{-0.36} \times 10^{52}$	$6.9^{+1.5}_{-1.2} \times 10^{52}$

Notes. Reported uncertainties correspond to 1σ confidence.
[a] Inferred circumburst densities as determined from afterglow observations (Fong et al. 2015).
[b] Maximum energy of a magnetar allowed by the observations assuming $\epsilon_B = 0.1$.

observations were taken at 1.425 GHz on timescales of $\delta t_{\rm rest} \approx 0.5$–2 yr. They detected no radio emission to 3σ limits of $\approx$200–500 μJy (Metzger & Bower 2014). A second study targeted two short GRBs with claims of associated kilonovae, GRB 060614 (Jin et al. 2015; Yang et al. 2015) and GRB 130603B (Berger et al. 2013; Tanvir et al. 2013), and detected no radio emission to 3σ limits of $\approx$150 and $\approx$60 μJy at rest-frame times of $\approx$7.9 and $\approx$1.3 yr, respectively (Horesh et al. 2016). With flux limits of $\lesssim$18–32 μJy for nine short GRBs, our study represents the deepest and most extensive campaign for late-time radio emission following short GRBs to date.

To demonstrate the improvement upon previous samples, we compile the rotational energy–circumburst density constraints for the nine bursts in our sample for $\epsilon_B = 0.1$ and the two ejecta masses, $M_{\rm ej} = 0.03\,M_\odot$ and $0.1\,M_\odot$ (Figure 4), and compare these to the corresponding constraints from the two previous studies (Metzger & Bower 2014; Horesh et al. 2016). We use the previously published radio limits, and assume the

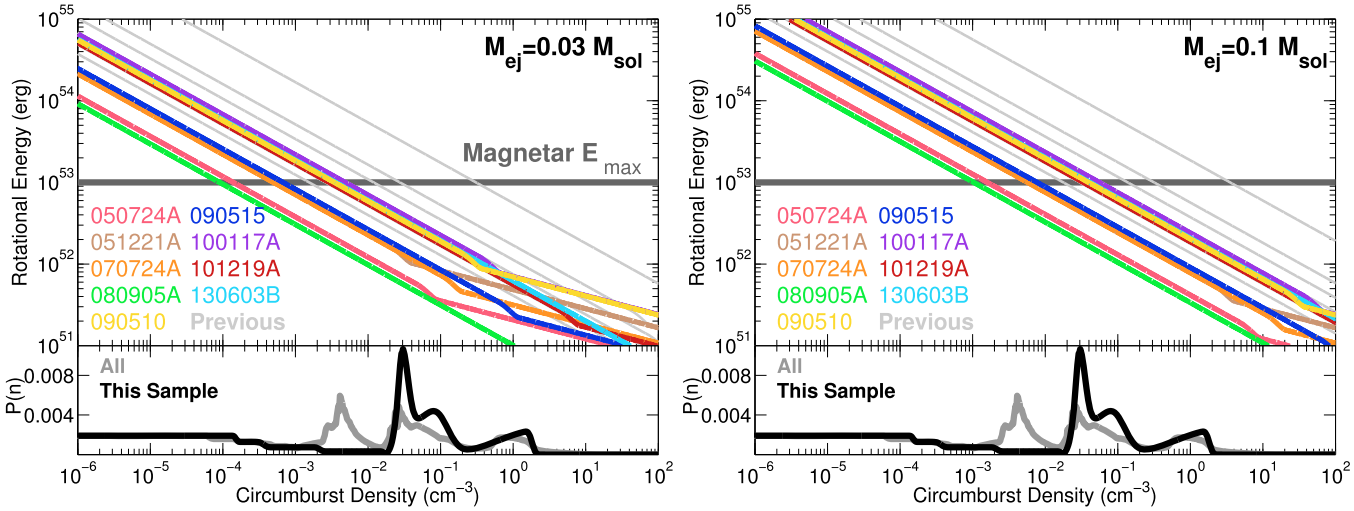

Figure 4. Constraints on the rotational energy–circumburst density parameter space from VLA observations for the nine short GRBs in our sample (colored curves) for $M_{\rm ej} = 0.03\,M_\odot$ (left) and $M_{\rm ej} = 0.1\,M_\odot$ (right), assuming $\epsilon_e = \epsilon_B = 0.1$ and $p = 2.4$. The curves represent upper limits on the parameter space, where the region below each curve is allowed and the region above is ruled out. Light gray curves denote constraints from previous work (Metzger & Bower 2014; Horesh et al. 2016). A gray horizonal line represents the maximum extractable rotational energy of a $\sim$2.2 $M_\odot$ magnetar of 10^{53} erg. In order to accommodate a magnetar with energy 10^{53} erg, the radio upper limits require that the circumburst densities are $\lesssim 4.8 \times 10^{-3}$ cm^{-3} ($\lesssim$0.06 cm^{-3}) for ejecta masses of 0.03 $M_\odot$ (0.1 $M_\odot$). Bottom panels show the distribution of densities as determined from afterglow observations for all short GRBs (gray) and for the bursts in this sample (black), where measurements have been weighted by their individual uncertainties.

same values for p, ϵ_e, and ϵ_B as in our study to ensure a uniform comparison. The resulting constraints are shown in Figure 4. The observations presented in this work provide deeper constraints on the combination of rotational energy and circumburst density by factors of $\approx$20–50. For instance, for lower ejecta masses, previous works are able to rule out a magnetar with an available energy reservoir of 10^{53} erg for circumburst densities of $\gtrsim$(1.5–250) $\times\ 10^{-3}$ cm^{-3}, compared to $\gtrsim$(0.09–4.8) $\times\ 10^{-3}$ cm^{-3} in this work (Figure 4). Also shown are the distributions of short GRB circumburst densities as inferred from their afterglows, for the nine bursts in this sample as well as the entire population. Overall, the large majority of short GRBs have low inferred densities of $\lesssim$0.1–1 cm^{-3} (Figure 4; Fong et al. 2015). Thus, in comparison to previous studies, our work provides more meaningful limits in the density regime that actually corresponds to the inferred densities of short GRBs.

Incorporating these circumburst density measurements from the afterglows, we place limits on the maximum energy of a long-lived magnetar remnant of $\lesssim$(0.02–17) $\times\ 10^{53}$ erg for lower ejecta masses, and $\lesssim$(0.05–55) $\times\ 10^{53}$ erg for higher ejecta masses. Overall, our observations rule out a magnetar energy of 10^{53} erg for half of the events in our sample. Thus, we can rule out the presence of an *indefinitely* stable magnetar in a significant fraction of short GRBs with anomalous X-ray behavior. However, we cannot rule out a relatively long-lived supramassive NS in these cases, which could survive for times approaching the magnetic dipole spin-down timescale (Spitkovsky 2006),

$$t_{\rm sd} \simeq 7\left(\frac{B_d}{10^{15}\ {\rm G}}\right)^{-2}\left(\frac{P}{1\ {\rm ms}}\right)^{2}\ {\rm hr}, \quad (4)$$

where P is the initial spin period and B_d is the dipole surface magnetic field strength of the magnetar.

Our observations rule out a magnetar with an energy reservoir of 10^{52} erg associated with a single event, GRB 050724A, which has a maximum allowed energy of $E_{\rm max} \approx$ (2–5) $\times\ 10^{51}$ erg (Table 2). This event exhibited extended emission in the X-ray band which has previously been attributed to the spin-down energy of a long-lived magnetar (Gompertz et al. 2013). If the merger that produced GRB 050724A resulted in a remnant NS with a typical mass of $M_{\rm ns} \approx 2.3$–$2.4\,M_\odot$ (e.g., Belczynski et al. 2008, their Figure 4), this would imply that the NS EOS must be relatively soft at high densities, such that it supports a maximum (non-rotating) NS mass of $\lesssim 2.2\,M_\odot$. This limit is also also supported by constraints from observations of radio pulsars (e.g., Ozel & Freire 2016).

If a remnant NS is responsible for the extended X-ray emission of GRB 050724A and the NS EOS is indeed soft, the remnant NS could be on the high mass end of the supramassive range ($\gtrsim 2.5\,M_\odot$), such that it imparts a relatively small amount of rotational energy of $\lesssim 5 \times 10^{51}$ erg to the surrounding medium before collapsing to a BH. In this case, the collapse time would be significantly less than the dipole spin-down timescale. By fitting the extended X-ray emission to a magnetar model, Gompertz et al. (2013) derived an initial spin period of $P \approx 2.2$ ms and magnetic field strength of $B_d \approx 2.1 \times 10^{16}$ G, giving a dipole spin-down timescale of $t_{\rm sd} \approx 270$ s (Equation (4)), which is indeed longer than the observed timescale of extended emission of $\approx$200 s.

We note that the above conclusions are dependent on the value of ϵ_B, and a very low value of ϵ_B would result in less stringent constraints on the energy of a magnetar. Our observational constraints would also be weakened if a large fraction of the magnetar rotational energy is emitted as gravitational waves instead of through electromagnetic spin-down (e.g., Doneva et al. 2015; Gao et al. 2016; Lasky & Glampedakis 2016). This could occur either due to a misalignment between the rotation axis and the magnetic dipole axis (e.g., Dall'Osso et al. 2009) or via the growth of the f-mode instability (e.g., Doneva et al. 2015). However,

gravitational-wave losses through these channels will probably only dominate the total spin-down rate if the internal toroidal magnetic field is two orders of magnitude larger than the external dipole field.

We compare our results to studies of magnetar emission from short GRBs at other wavelengths. Gompertz et al. (2015) used a broadband afterglow model with time-varying energy injection due to spin-down of a long-lived magnetar to fit the X-ray and optical emission of four short GRBs with X-ray plateaus, and made predictions for the associated radio emission. For the two events that overlap with our sample, GRBs 051221A and 130603B, the predicted radio emission is $\lesssim 1\ \mu$Jy at GHz frequencies at $\gtrsim$100 days after the burst (Gompertz et al. 2015), consistent with the limits in this paper. Similarly, fits to the luminosity and duration of short GRB X-ray plateaus with the magnetar model resulted in $\approx(0.01\text{–}6) \times 10^{52}$ erg of energy emitted during the plateau phase (Rowlinson et al. 2013), consistent with the values of $E_{\rm max}$ from our studies. In addition, Rowlinson et al. (2013) find that ≈50% of events form unstable magnetars. In order to accommodate both the early-time X-ray activity and the limits on the long-term radio emission, we conclude that supramassive magnetars that inject a total energy of $\lesssim 10^{53}$ erg must be relatively common compared to stable magnetars. Using a large sample of X-ray afterglow light curves, Lü et al. (2015) came to the similar conclusion that NS mergers likely result in supramassive NSs. If the total energy constraints from our observations were uniformly more stringent, $\lesssim 10^{52}$ erg, the collapse to a BH should be relatively abrupt (i.e., during the plateau phase itself), and we would expect more events with dramatic drops in their X-ray light curves, similar to GRB 090515 (Rowlinson et al. 2010a).

We note that the radio emission model (Section 3) applied in this paper neglects relativistic effects, both on the ejecta dynamics and the emission (e.g., relativistic Doppler beaming). To understand how this simplification affects our results, we generate light curve models for the parameters considered by Horesh et al. (2016), who interpolate their results to also consider the relativistic limit. We find that for models with ejecta mass of $0.1\ M_\odot$, the peak fluxes and timescales are virtually identical across the full range of densities and energies considered here. However, for a lower ejecta mass of $0.01\ M_\odot$, the peak fluxes are elevated by a factor of ≈10, and the deceleration timescales are shortened by a factor of ≈2–3 when compared to the Newtonian case. Therefore, incorporating relativistic effects only serves to make the predicted emission brighter, which then makes our observations even more constraining.

6. CONCLUSIONS

We study the long-term radio behavior of nine short GRBs with early-time excess emission in the X-ray band, which may signify the presence of magnetars. Through our VLA observations on rest-frame timescales of ≈2–8 yr after the bursts, we find no radio emission to luminosity limits of $\lesssim(0.05\text{–}8) \times 10^{39}$ erg s^{-1} at 6.0 GHz. Our study demonstrates that a significant fraction of short GRBs with anomalous X-ray behavior do not have the associated radio emission predicted from long-lived magnetars with energy reservoirs of 10^{53} erg. We also rule out a stable magnetar with an energy reservoir of 10^{52} erg in a single case, GRB 050724A. These radio observations, together with the known X-ray behavior, imply that supramassive magnetars which inject $\lesssim 10^{53}$ erg of energy are common relative to stable magnetars.

Our study shows that a stiff NS EOS, corresponding to a maximum stable (non-rotating) NS mass of $M_{\rm ns} \gtrsim 2.3\text{–}2.4\ M_\odot$, is disfavored, unless the NS mergers that give rise to short GRBs are particularly massive. However, population synthesis models suggest that such massive binaries only comprise a small fraction of all NS mergers (Belczynski et al. 2008). A comparison of the observed rate of short GRBs to constraints on the NS merger rate from Advanced LIGO/Virgo will soon provide insight on the fraction of NS mergers that give rise to short GRBs, and thus additional insight into the NS EOS (e.g., Fryer et al. 2015). Upcoming wide-field radio surveys will also constrain the population of long-lived magnetars (Metzger et al. 2015), independent of an association with short GRBs.

We cannot rule out that a long-lived magnetar is responsible for the extended X-ray activity after some short GRBs. However, we can conclude that most such remnants should be supramassive and hence should collapse to black holes on timescales that are comparable to or shorter than their magnetic dipole spin-down timescales. If future radio observations can uniformly constrain the total available energy from a magnetar to $\lesssim 10^{52}$ erg, we should expect more abrupt collapse signatures in the X-ray light curves of short GRB afterglows.

The lack of evidence for stable, long-lived magnetars may impact observational signatures from NS mergers at other wavelengths. For example, neutron-rich outflows from the NS merger form heavy elements via the *r*-process and undergo radioactive decay, resulting in a kilonova transient (Li & Paczyński 1998). In the absence of a long-lived magnetar, the signal is expected to peak in the near-IR band on ∼week timescales due to the large opacities of the heavy elements produced (Barnes & Kasen 2013; Kasen et al. 2013; Tanaka & Hotokezaka 2013; Grossman et al. 2014; Fontes et al. 2015). In contrast, the large neutrino luminosity from a long-lived magnetar may inhibit the formation of very heavy elements, resulting in a bluer kilonova that peaks at optical wavelengths on ∼day timescales (Metzger & Fernández 2014; Kasen et al. 2015). If the sample in this paper is representative of all NS mergers, this supports the idea that kilonovae associated with NS mergers peak in the redder bands.

Since NS mergers are expected to be strong sources of gravitational waves, similar searches for long-term radio emission following NS mergers detected within the Advanced LIGO/Virgo horizon distance of 200 Mpc will be able to place limits of $\lesssim 6 \times 10^{36}$ erg s^{-1}. Thus, such searches will be crucial in constraining the fraction of mergers that lead to magnetars with delayed or no collapse to a black hole to significantly higher confidence than is possible with the cosmological sample.

Support for this work was provided by NASA through Einstein Postdoctoral Fellowship grant number PF4-150121. B.D.M. gratefully acknowledges support from NASA Fermi grant NNX14AQ68G, NSF grant AST-1410950, NASA ATP grant NNX16AB30G, and the Alfred P. Sloan Foundation. E.B. acknowledges support from NSF grant AST-1411763 and NASA ADA grant NNX15AE50G. The National Radio Astronomy Observatory is a facility of the National Science Foundation operated under cooperative agreement by Associated Universities, Inc.

REFERENCES

Aloy, M. A., Janka, H.-T., & Müller, E. 2005, A&A, 436, 273
Antoniadis, J., Freire, P. C. C., Wex, N., et al. 2013, Sci, 340, 448
Arras, P., Flanagan, E. E., Morsink, S. M., et al. 2003, ApJ, 591, 1129
Barnes, J., & Kasen, D. 2013, ApJ, 775, 18
Belczynski, K., O'Shaughnessy, R., Kalogera, V., et al. 2008, ApJL, 680, L129
Berger, E. 2009, ApJ, 690, 231
Berger, E. 2010, ApJ, 722, 1946
Berger, E. 2014, ARA&A, 52, 43
Berger, E., Fong, W., & Chornock, R. 2013, ApJL, 774, L23
Berger, E., Price, P. A., Cenko, S. B., et al. 2005, Natur, 438, 988
Bucciantini, N., Metzger, B. D., Thompson, T. A., & Quataert, E. 2012, MNRAS, 419, 1537
Cannizzo, J. K., Troja, E., & Gehrels, N. 2011, ApJ, 734, 35
Cucchiara, A., Prochaska, J. X., Perley, D., et al. 2013, ApJ, 777, 94
Dall'Osso, S., Shore, S. N., & Stella, L. 2009, MNRAS, 398, 1869
de Ugarte Postigo, A., Thöne, C. C., Rowlinson, A., et al. 2014, A&A, 563, A62
Demorest, P. B., Pennucci, T., Ransom, S. M., Roberts, M. S. E., & Hessels, J. W. T. 2010, Natur, 467, 1081
Doneva, D. D., Kokkotas, K. D., & Pnigouras, P. 2015, PhRvD, 92, 104040
Duncan, R. C., & Thompson, C. 1992, ApJL, 392, L9
Fan, Y.-Z., Yu, Y.-W., Xu, D., et al. 2013, ApJL, 779, L25
Fernández, R., & Metzger, B. D. 2013, MNRAS, 435, 502
Fong, W., & Berger, E. 2013, ApJ, 776, 18
Fong, W., Berger, E., Margutti, R., & Zauderer, B. A. 2015, ApJ, 815, 102
Fong, W., Berger, E., Chornock, R., et al. 2011, ApJ, 730, 26
Fong, W., Berger, E., Chornock, R., et al. 2013, ApJ, 769, 56
Fong, W., Berger, E., Metzger, B. D., et al. 2014, ApJ, 780, 118
Fontes, C. J., Fryer, C. L., Hungerford, A. L., et al. 2015, HEDP, 16, 53
Fryer, C. L., Belczynski, K., Ramirez-Ruiz, E., et al. 2015, ApJ, 812, 24
Gao, H., Zhang, B., & Lü, H.-J. 2016, PhRvD, 93, 044065
Gehrels, N., Chincarini, G., Giommi, P., et al. 2004, ApJ, 611, 1005
Giacomazzo, B., & Perna, R. 2013, ApJL, 771, L26
Gompertz, B. P., O'Brien, P. T., Wynn, G. A., & Rowlinson, A. 2013, MNRAS, 431, 1745
Gompertz, B. P., van der Horst, A. J., O'Brien, P. T., Wynn, G. A., & Wiersema, K. 2015, MNRAS, 448, 629
Greisen, E. W. 2003, Information Handling in Astronomy—Historical Vistas, Vol. 285 (Dordrecht: Kluwer Academic Publishers)
Grossman, D., Korobkin, O., Rosswog, S., & Piran, T. 2014, MNRAS, 439, 757
Horesh, A., Hotokezaka, K., Piran, T., Nakar, E., & Hancock, P. 2016, ApJL, 819, L22
Hotokezaka, K., Kiuchi, K., Kyutoku, K., et al. 2013a, PhRvD, 87, 024001
Hotokezaka, K., Kyutoku, K., Tanaka, M., et al. 2013b, ApJL, 778, L16
Hotokezaka, K., & Piran, T. 2015, MNRAS, 450, 1430
Jin, Z.-P., Li, X., Cano, Z., et al. 2015, ApJL, 811, L22
Just, O., Bauswein, A., Pulpillo, R. A., Goriely, S., & Janka, H.-T. 2015, MNRAS, 448, 541
Kasen, D., Badnell, N. R., & Barnes, J. 2013, ApJ, 774, 25
Kasen, D., Fernández, R., & Metzger, B. D. 2015, MNRAS, 450, 1777
Kumar, P., Narayan, R., & Johnson, J. L. 2008, MNRAS, 388, 1729
Kyutoku, K., Ioka, K., Okawa, H., Shibata, M., & Taniguchi, K. 2015, PhRvD, 92, 044028
Lasky, P. D., & Glampedakis, K. 2016, MNRAS, 458, 1660
Lasky, P. D., Haskell, B., Ravi, V., Howell, E. J., & Coward, D. M. 2014, PhRvD, 89, 047302
Lawrence, S., Tervala, J. G., Bedaque, P. F., & Miller, M. C. 2015, ApJ, 808, 186
Li, L.-X., & Paczyński, B. 1998, ApJL, 507, L59
Lü, H.-J., Zhang, B., Lei, W.-H., Li, Y., & Lasky, P. D. 2015, ApJ, 805, 89
Margutti, R., Chincarini, G., Granot, J., et al. 2011, MNRAS, 417, 2144
Margutti, R., Zaninoni, E., Bernardini, M. G., et al. 2013, MNRAS, 428, 729
McBreen, S., Krühler, T., Rau, A., et al. 2010, A&A, 516, A71
Metzger, B. D., & Bower, G. C. 2014, MNRAS, 437, 1821
Metzger, B. D., & Fernández, R. 2014, MNRAS, 441, 3444
Metzger, B. D., Margalit, B., Kasen, D., & Quataert, E. 2015, MNRAS, 454, 3311
Metzger, B. D., & Piro, A. L. 2014, MNRAS, 439, 3916
Metzger, B. D., Piro, A. L., & Quataert, E. 2009, MNRAS, 396, 304
Metzger, B. D., Quataert, E., & Thompson, T. A. 2008, MNRAS, 385, 1455
Metzger, B. D., Williams, P. K. G., & Berger, E. 2015, ApJ, 806, 224
Nakar, E., & Piran, T. 2011, Natur, 478, 82
Narayan, R., Paczynski, B., & Piran, T. 1992, ApJL, 395, L83
Norris, J. P., & Bonnell, J. T. 2006, ApJ, 643, 266
Özel, F., Baym, G., & Güver, T. 2010, PhRvD, 82, 101301
Ozel, F., & Freire, P. 2016, ARA&A, 54, 401
Özel, F., Psaltis, D., Güver, T., et al. 2016, ApJ, 820, 28
Özel, F., Psaltis, D., Ransom, S., Demorest, P., & Alford, M. 2010, ApJL, 724, L199
Perley, D. A., Metzger, B. D., Granot, J., et al. 2009, ApJ, 696, 1871
Price, D. J., & Rosswog, S. 2006, Sci, 312, 719
Radice, D., Galeazzi, F., Lippuner, J., et al. 2016, MNRAS, 460, 3255
Rezzolla, L., Giacomazzo, B., Baiotti, L., et al. 2011, ApJL, 732, L6
Rosswog, S. 2007, MNRAS, 376, L48
Rosswog, S., Liebendörfer, M., Thielemann, F.-K., et al. 1999, A&A, 341, 499
Rowlinson, A., O'Brien, P. T., Metzger, B. D., Tanvir, N. R., & Levan, A. J. 2013, MNRAS, 430, 1061
Rowlinson, A., O'Brien, P. T., Tanvir, N. R., et al. 2010a, MNRAS, 409, 531
Rowlinson, A., Wiersema, K., Levan, A. J., et al. 2010b, MNRAS, 408, 383
Ruffert, M., & Janka, H.-T. 1999, A&A, 344, 573
Ruiz, M., Lang, R. N., Paschalidis, V., & Shapiro, S. L. 2016, ApJL, 824, L6
Shibata, M., & Taniguchi, K. 2006, PhRvD, 73, 064027
Siegel, D. M., & Ciolfi, R. 2016, ApJ, 819, 14
Siegel, D. M., Ciolfi, R., & Rezzolla, L. 2014, ApJL, 785, L6
Soderberg, A. M., Berger, E., Kasliwal, M., et al. 2006, ApJ, 650, 261
Spitkovsky, A. 2006, ApJL, 648, L51
Tanaka, M., & Hotokezaka, K. 2013, ApJ, 775, 113
Tanvir, N. R., Levan, A. J., Fruchter, A. S., et al. 2013, Natur, 500, 547
Tunnicliffe, R. L., Levan, A. J., Tanvir, N. R., et al. 2014, MNRAS, 437, 1495
Usov, V. V. 1992, Natur, 357, 472
Yang, B., Jin, Z., Li, X., et al. 2015, NatCo, 6, 7323
Zhang, B., & Mészáros, P. 2001, ApJL, 552, L35
Zrake, J., & MacFadyen, A. I. 2013, ApJL, 769, L29